Journal of Alloys and Compounds 488 (2009) 31–34

Contents lists available at ScienceDirect

Journal of Alloys and Compounds

journal homepage: www.elsevier.com/locate/jallcom

Giant dielectric permittivity in Li and Pr co-doped NiO ceramics

A.A. Dakhel*

Dept. of Physics, College of Science, University of Bahrain, P.O. Box 32038, Bahrain

ARTICLE INFO

Article history:
Received 7 July 2009
Received in revised form 26 August 2009
Accepted 27 August 2009
Available online 8 September 2009

PACS:
77.22.Ch
77.22.Gm
77.84.Bw
91.60.Ed

Keywords:
Ceramics
Dielectrics
Dielectric properties
Electrical properties
Grain boundaries
NiO

ABSTRACT

The objective of the present work is to use rare-earth oxide (Pr oxide) as dopant to Li-doped NiO ceramics in order to obtain giant dielectric permittivity (ε') together with low loss factor ($\tan\phi$). For that aim, NiO-based ceramics of a formula $Li_xPr_yNi_{1-x-y}O$ (LPNO) with $x = 0.027$ and $y = 0.001$ and 0.005 have been synthesized by usual solid-state reaction. Their structural characterization was carried out with X-ray diffraction (XRD) and X-ray fluorescence (XRF). Their bulk dielectric properties at room temperature have been studied in detail. A giant low-frequency dielectric permittivity ($\varepsilon' \sim 10^5$–10^6) together with a low loss factor ($\tan\delta \sim 0.05$–0.08) at room temperature was obtained. The giant values from dielectric permittivity were explained in the framework of core/shell model and the low loss factor was explained by the formation of grain boundaries rich with Pr oxide. Complex-impedance study shows a non-Debye type relaxation in the LPNO compounds. In general, the results of the present work suggest adopting doping with rare earths in low concentrations in order to obtain giant dielectric permittivity together with low loss factor.

1. Introduction

NiO-based ceramics of a formula $A_xB_yNi_{1-x-y}O$ (where A stands for a monovalent element such as Li, Na, K and B stands for a transition element like Ti, Fe, V, Ta, Al [1–5]) have attracted a considerable attention due to their very high (giant) apparent dielectric permittivity (10^3–10^5) together with a non-perovskite and non-ferroelectric properties. The permittivity (ε') of such materials remains constant in the temperature range around room temperature, −50 to 150 °C [1,6]. In addition the giant permittivity remains almost constant at low frequencies, then it rapidly decreases for sufficiently high frequencies [1,3,4,7]. The giant permittivity of such materials was explained by application of Maxwell–Wagner (M–W) or interfacial polarization model [8]. In this model, the giant dielectric polarization is resulted from the microstructural heterogeneous structure, which consists of grains and grain boundaries. The grain substance has a semiconducting properties and the grain boundaries (GBs) have an insulating properties [1,7,6,9]. Therefore, by application of an electric field, the free charge carriers in the semiconducting grain are accumulated at the two edge sides of insulating GB thin-layers, producing strong interfacial polarization at the this boundary-layer capacitors (BLCs). This is responsible for the observation of high-ε due to small thickness of the GB, as proposed by Wu et al. [1]. However, such explanation is still under investigation and needs more data base, which is also necessary before practical applications in devices that need giant-ε and low dielectric loss ($\tan\delta$). However, the usually obtained loss factor for such ceramics is high except in case of $K_{0.05}Ti_{0.02}Ni_{0.93}O$ (KTNO) ceramic that exhibits high-ε and low $\tan\delta$ [4,10]. It is known that the dielectric loss for these ceramics can be lowered by increase in the resistance of GBs through changing the compositions of the additives of A and B that tuned the dielectric properties [1,6]. Thus, in this paper, we use Pr as B-element because Pr oxide has high dielectric permittivity (among other rare-earth oxides) and good insulating properties. Furthermore, Pr (and other rare earths) has generally low solid solubility in NiO (analogues to ZnO [11,12]) mainly due to the ionic sizes. The Pr^{3+} ion (0.1013 nm) is much larger than Ni^{2+} (0.069 nm) [13] therefore, incorporation of Pr^{3+} ion in NiO matrix would cause a big lattice distortion. For that reason, one can expect that Pr oxide should mainly accumulate on grain boundaries and thus enhances the isolation between grains and reduces the dielectric loss. In this work we study, for the first time, the structural and electrical properties of $Li_xPr_yNi_{1x-y}O$ ceramics, where $x = 0.027$ and $y = 0.001$ and 0.005. We will see that these ceramics are oxides of giant dielectric permittivity, non-perovskite structure, and have non-ferroelectric or paramagnetic

* Fax: +973 17449148.
E-mail address: adakhil@sci.uob.bh.

0925-8388/$ – see front matter © 2009 Elsevier B.V. All rights reserved.
doi:10.1016/j.jallcom.2009.08.155

properties at room temperature. The results of the present work will be explained within the framework of the core/shell model i.e. electrically heterogeneous microstructure is responsible for the observed giant-ε. The Li^+ ions doped into NiO matrix induces transformation of some Ni^{2+} ions into Ni^{3+}, which convert pure NiO into semiconductor meanwhile the transition metal dopant (like Ti, V, or W [1,6,14]) is mainly accumulates on the grain boundaries. Thus the interior of the grains is a semiconductor (mainly Li-doped NiO) while the shell of the grains is a transition metal-rich insulating boundaries.

2. Experimental details

In this work, NiO, $Li(OH)\cdot H_2O$ and Pr_6O_{11} (Fluka A.G.) were used as starting materials. Stoichiometric amounts of starting material powders were well mixed by an agate mortar and pestle, and calcinated in air at 1000 °C for about 20 h. Then, the yield powder was pressed (750 MPa) into pellets 1–2 mm in thickness. Finally, these pellets were sintered at 1300 °C for about 20 h. The obtained ceramic samples (abbreviated as LPNO ceramic) were denoted as: LPNO-1 for $Li_{0.030}Pr_{0.001}Ni_{0.969}O$ and LPNO-2 for $Li_{0.030}Pr_{0.005}Ni_{0.965}O$ in addition to NiO:Li that is $Li_{0.03}Ni_{0.97}O$. The undoped NiO that passed the same calcination procedure was used as a reference. For electrical measurements, aluminum thin film electrodes were vacuum deposited on both faces of disc-shaped samples. For elemental analysis of the samples, the energy dispersion X-ray fluorescence (EDXRF) spectroscopy method was used. The exciting radiation was Cu K_α and the detector was an Amptek XR-100CR detector. For the structural analysis, the X-ray diffraction (XRD) method was used with a Philips PW-1710 θ–2θ system with Cu K_α radiation (0.15406 nm) and a step size of 0.02°. The dielectric and electrical responses were measured using a Keithley 3330 LCZ instrument, hp 4275A LCR meter, and Keithley model 6487 picoammeter. The measuring frequency range was 100 Hz to 200 kHz with signal voltage 50 mV.

3. Structural characterization

Fig. 1 shows the energy dispersion XRF spectrum of the prepared NiO:Li and LPNO ceramic samples. The spectrum shows Ni K_α(7.47 keV), Pr L_α (5.03 keV), Pr $L_{\beta1}$ (5.48 keV), and signal from the Cu source of the X-ray tube. The signals from lithium and oxygen cannot be detected with the used detector. No other significant signals were detected.

The XRD patterns of samples NiO:Li, LPNO-1, and LPNO-2 are depicted in Fig. 2 together with that of the reference undoped NiO pressed disc. All samples exhibit a phase of NiO. The reference undoped NiO has a cubic FCC (Fm3m) structure with lattice constant 0.42 nm, which is almost identical with the standard a = 0.4172 nm [15]. The (2 0 0) reflection of NiO has the highest intensity, as that of the standard diffraction pattern. Doping of NiO matrix with lithium Li ions (sample NiO:Li) is considerably increases Bragg positions (2θ) of the reflections (Table 1). This signs

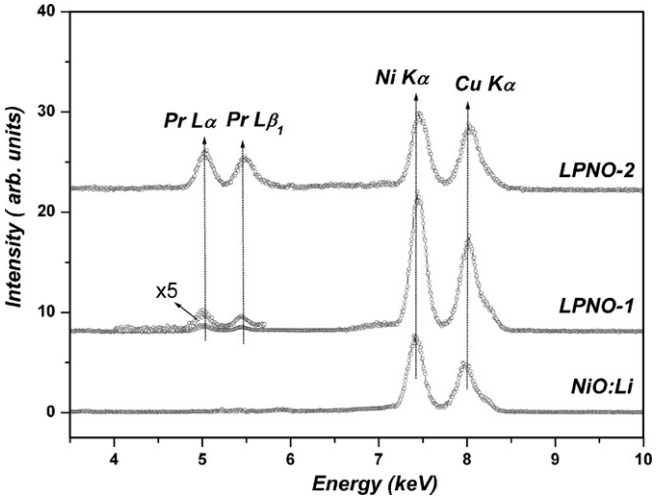

Fig. 1. Corrected XRF spectrum of NiO:Li, LPNO-1, and LPNO-2 ceramics. The exciting radiation was Ni-filtered Cu K_α radiation.

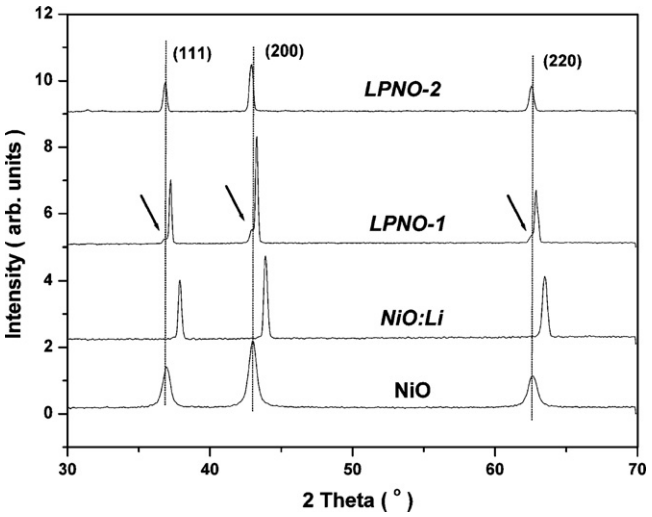

Fig. 2. XRD patterns of NiO, NiO:Li, LPNO-1, and LPNO-2 ceramics. The radiation used was Cu K_α-line.

to a decrease in the NiO lattice parameter by about 1.6%; such fact was also observed in other works of Refs. [16,17] and was explained by the substitution of Ni^{2+} sites with Li^+ ions, which have smaller radius of 0.068 nm. The XRD of LPNO-1 shows a mixture of two cubic structures different slightly by lattice parameter, one is NiO and the other is Li-doped NiO. For praseodymium, due to its very small solid solubility in NiO, one can expect that it mainly accumulates on GBs; identical explanation was also given in works of Refs. [1,10,14] on transition metals (Ti, V, W) and Al, and observed directly in Ref. [6] by using scanning electron microscope (SEM). (It must be mentioned here that such accumulation makes the samples inhomogeneous that was observed and supported by the measurements of the ac-electrical properties in Section 4.) This accumulation gradually inhibits the doping of Li into NiO matrix i.e. gradually inhibits the formation of NiO:Li. The XRD of LPNO-2 shows a single NiO-structure phase, identified to be of NiO grains slightly affected by the presence of impurities of Pr and Li. Any crystalline second phase was not detected in the present investigation (the second phase might exist in a very small undetectable quantity). Thus, LPNO-2 sample consists of mainly NiO grains surrounding by boundaries, which contains Pr-, Ni-, and Li-oxides in amorphous state, that have no observable effect on the obtained XRD profile (like humps) due to its very small amount. Therefore, the investigated sample has heterogeneous core/shell structure containing NiO (for LPNO-2) or mainly Li-doped NiO (for LPNO-1) grains and insulating Pr-, Ni- and Li-oxide rich boundary layer; analogous to other giant dielectric permeability doped NiO [1,6,14].

The average X-ray grain size (GS) given in Table 1 was calculated by Scherer's relation [18] using the intense (2 0 0) reflection of NiO-structure. The NiO grains grow in size due to the Li doping (sample NiO:Li) that improve the crystallinity of the sample, as also observed in Ref. [19]. The grain growth continued with addition of Pr as in LPNO-1, and then followed by decreasing with more addition of Pr as in sample LPNO-2. This peak shift $\Delta(2\theta_{200})$ is resulted

Table 1
X-ray Bragg angle ($2\theta_{200}$, °) for (2 0 0) reflection and its half-width ([2θ°]), average XR-grain size (GS), microstrain (ε_s), and structural stress (σ_{st}) for the prepared reference pure NiO and NiO doped with Li and Pr (LPNO ceramics).

Sample	$2\theta_{200}$°	[2θ°]	GS (nm)	ε_s (10^{-3})	σ_{st} (GPa)
NiO	43.09	0.52	16.5	–	–
NiO:Li	43.86	0.32	27.0	−16.7	6.9
LPNO-1	43.27	0.16	53.8	−3.9	1.6
LPNO-2	42.96	0.32	26.8	+2.8	1.2

from of a created strain ($\varepsilon_s = -\Delta\theta_{(101)}\cot\theta_{(101)}$), which is of order ($10^{-2}$ to 10^{-3}) with estimated accuracy of $\pm 1.7 \times 10^{-3}$. This strain is caused by a compressive (for negative sign) microstress (σ_{st}) that can be estimated by: $\sigma_{st} \approx (3\varepsilon_s)B$, where B is the average bulk modulus of NiO, which is about 138.3 GPa [20]. Values of ε_s and σ_{st} are given in Table 1, where one can conclude that compressive stress created in NiO-structure by Li^+ doping is removed gradually with reduction of Li doping due to Pr addition.

4. Dielectric and electric properties at room temperature

It is known that normal, pure, and stoichiometric NiO is a Mott–Hubbard insulator at room temperature of a very low electrical conductivity about 10^{-13} S/cm [1]. Creation of Ni^{2+} vacancies disturb its lattice locally and transform it into p-type semiconductor [1]. p-Type semiconducting behaviour of NiO can be boosted by doping with monovalent cations such as Li^+, similar to that of an acceptor impurity function [19]. However, the conductivity of a pressed reference NiO disc in the present work is 4.23×10^{-7} S/cm, which is close to the range (10^{-1} to 10^{-6} S/cm) usually found experimentally by many researchers [19]. This means that the calcination of the reference NiO creates structural Ni^{2+} vacancies that improve the conductivity. The dc-electrical conductivity of NiO is more improved with Li^+-doping becoming 4.76×10^{-4} S/cm at room temperature for NiO:Li sample of the present work. Thus with a little Li doping ($Li_{0.027}Ni_{0.973}O$), a considerable increase in its conductivity takes place, in agreement with the results of Refs. [1,18,19] obtained from NiO:Li thin film. The dc-conductivity of LPNO-1 was 3.34×10^{-6} S/cm and of LPNO-2 was 9.1×10^{-4} S/cm.

The frequency dependent of dielectric properties of the NiO:Li and LPNOs samples measured in the range 100 Hz–200 kHz are shown in Fig. 3. The real part of the dielectric permittivity, ε', of LPNO samples shows giant values and constant until about 100 kHz where rapidly decreases. This behaviour is typical as for other NiO-based ceramic systems [1,3,4,6] and was explained by Maxwell–Wagner relaxation mechanism. The variation of Pr molar% has clear effect on ε' as well as on loss factor $\tan\delta$ (inset of Fig. 3). The giant-ε property was also observed in NiO:Li due to the Li^+ doping and GB effect. But the behaviour of $\varepsilon'(\omega)$ relationship of NiO:Li is different from that of LPNO ceramics, it decreases quickly by increasing of frequency. Thus the clear effect of Pr addition is to change the $\varepsilon'(\omega)$ relationship behaviour as well as to reduce the loss factor ($\tan\phi$), which is very important for practical applications as mentioned in the introduction section to be one of the goals of the present study. A minimum value of 0.05 was measured for LPNO-1 at 3 kHz increases to 0.07 at 10 kHz. Fig. 4 shows the effect of Pr addition to the prepared samples on the dielectric properties measured at 10 kHz. It is clear that accumulation of Pr oxide on the GBs increases the ε' and decreases $\tan\delta$ in such a way that it becomes the smallest for LPNO-1. Numerically the ε' and $\tan\delta$ values at 1 kHz are 6.08×10^5 and 0.08 for LPNO-1, and 1.0×10^6 and 0.3 for LPNO-2. These new giant data suggest adopting doping with rare earths with low concentrations in order to obtain giant-ε' together with low loss factor. It was observed that the values of ε' and $\tan\delta$ at 10 kHz are almost constant by increasing temperature to about 50 °C; such result was also observed for other NiO-based giant materials [1,10].

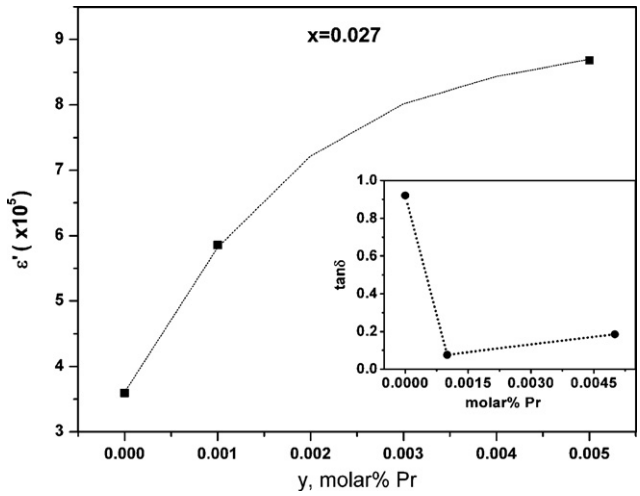

Fig. 4. Dependence of the dielectric permittivity, ε', and loss factor, $\tan\phi$ (the inset) measured at room temperature and 10 kHz on the Pr dopant molar fraction (y) in $Li_xPr_yNi_{1-x-y}O$ ceramics.

Complex-impedance spectroscopy method is usually used to characterise the electrical properties of materials and their interfaces with electronically conducting electrodes [21] or to separate out the bulk and GBs contributions [6]. Fig. 5 shows the frequency dependence of real part (Z') and imaginary part (Z'') of the complex impedance of the prepared samples. The relationship $Z''(\omega)$ is given in log–log scale in order to show the almost linear relationship. The obvious effect of Pr addition appears at low frequencies, which reflects the difference in the two kinds of the GBs (with and

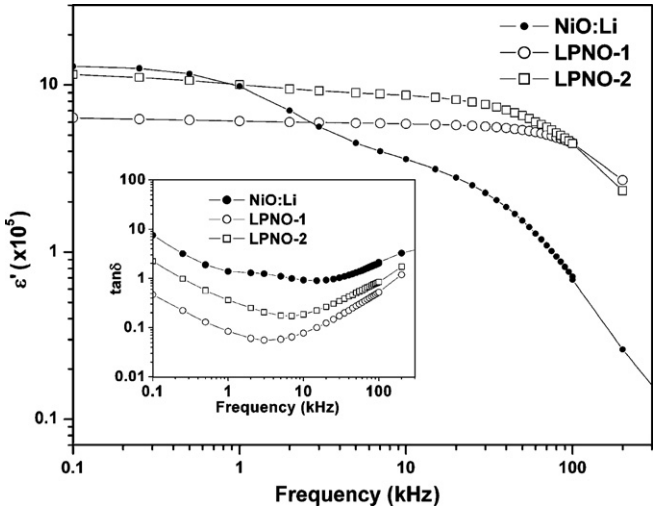

Fig. 3. Room temperature frequency dependence of dielectric permittivity, ε', of NiO:Li, LPNO-1, and LPNO-2 ceramics. The inset shows the frequency dependence of loss factor, $\tan\phi$, of the same samples.

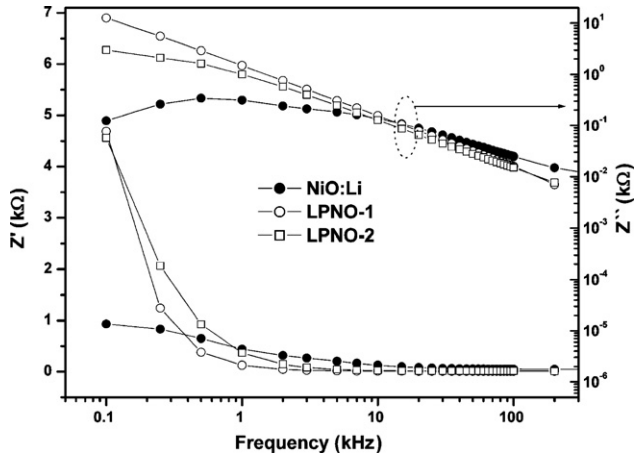

Fig. 5. Frequency dependence of real part (Z') and imaginary part (Z'') of the complex impedance measured at room temperature for NiO:Li, LPNO-1, and LPNO-2 ceramics.

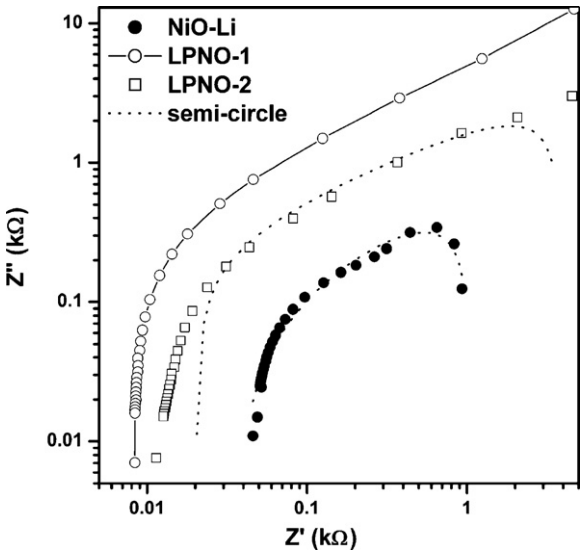

Fig. 6. Nyquist impedance plots (in log–log scale) measured at room temperature for NiO:Li, LPNO-1, and LPNO-2 ceramics. The dotted lines represent the theoretical semicircles.

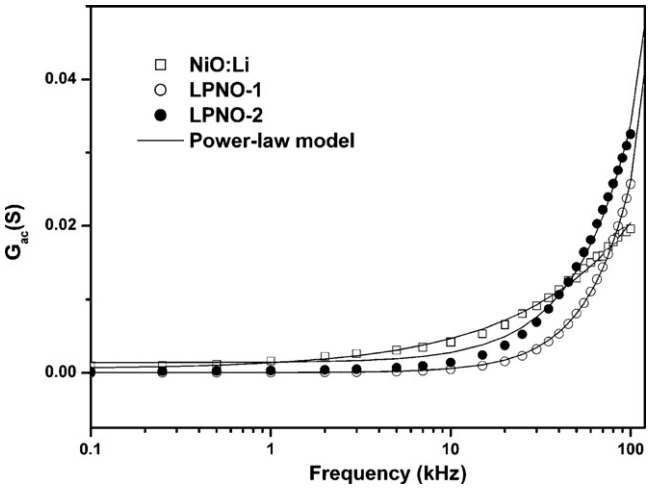

Fig. 7. Frequency dependence of ac-conductance (G_{ac}) measured at room temperature for NiO:Li, LPNO-1, and LPNO-2 ceramics. The lines represent the theoretical simulation according to the power-law model.

without Pr). Fig. 6 shows the Nyquist plots (in log–log scale) for the samples. One semi-circular arc (dotted line) is totally appropriate only for data of NiO:Li, while it is not suitable to describe all data points of LPNO samples. This can be explained that dielectric response in NiO:Li comes from one major mechanism while that of LPNO samples is due to more than one mechanisms, overlapped on each other at room temperature, which can be separated in the studied frequency range by raising the temperature during measurements (that is the subject of the future investigation).

Finally, the ac-conductivity is studied in the present work. The ac-conductance (G_{ac}) of insulators is often expressed according to the following relation: $G_{ac} = G_{dc}(0) + G_{ac}(\omega)$, where $G_{dc}(0)$ is the dc-conductance of the sample and $G_{ac}(\omega)$ is the frequency-dependent component. $G_{ac}(\omega)$ is typically expressed by a power law $G_{ac}(\omega) = A_\sigma \omega^s$, where A_σ is a coefficient [22]. According to the correlated barrier hopping (CBH) model, the exponent s is related to the maximum barrier height for hopping W_M that has any value less than energygap (E_g) and thus $s < 1$ [23]. W_M must depend on the film's microstructure like the average grain size, texture orientation, defect distribution, phase content, etc. However, none of these factors was entered into (CBH) model derived originally for uniform homogeneous non-crystalline insulators. Therefore, the experimental value of s could be any value <1 and also s could take values >1, as it was observed in some experimental results [24,25]. These results were explained due to the non-random distribution of hopping centres because of structural and defect distribution inhomogeneity [23], which causes enhancement of the frequency exponent "s" by an additional factor depends on the type of inhomogeneity in the insulator [23,26]. Fig. 7 shows the frequency dependence of ac-conductance $G(\omega)$. The application of the above model gives the following values for s: 0.67, 1.69, and 1.37 for NiO:Li, LPNO-1, and LPNO-2, respectively. According to the CBH model, these results clearly show the structural homogeneity of Li-doped NiO and with Pr addition, the LPNO structures become inhomogeneous.

5. Conclusions

It has been found that the Li and Pr co-doped NiO ceramics exhibit a giant low-frequency dielectric permittivity, $e' \sim 10^5$–10^6, together with low loss factor, $\tan\phi \sim 0.05$–0.07, which is slowly, varies with frequency till 100 kHz and almost temperature independent till 50 °C. Such giant dielectric permittivity was explained as consequence of the effect of the microstructural construction of the sample that theoretically studied in the framework of core/shell model. The low loss factor was explained by the accumulation of Pr oxide together with Li-oxide on the grain boundaries. The results of the present work suggest adopting doping with rare earths in low concentrations in order to obtain giant dielectric permittivity together with low loss factor.

References

[1] J. Wu, C.W. Nan, Y. Lin, Y. Deng, Phys. Rev. Lett. 89 (2002) 217601.
[2] S. Maensiri, P. Thongbai, T. Yamwong, Acta Mater. 55 (2007) 2851.
[3] Y. Lin, L. Jiang, R. Zhao, C.W. Nan, Phys. Rev. B 72 (2005) 014103.
[4] P.K. Jana, S. Sarkar, B.K. Chaudhuri, Appl. Phys. Lett. 88 (2006) 182901.
[5] P.K. Jana, S. Sarkar, H. Sakata, T. Watanabe, B.K. Chaudhuri, Phys. D: Appl. Phys. 41 (2008) 065403.
[6] S. Pongha, P. Thongbai, T. Yamwong, S. Maensiri, Scripta Mater. 60 (2009) 870.
[7] Y.H. Lin, J. Wang, l. Jiang, Y. Chen, C.W. Nan, Appl. Phys. Lett. 85 (2004) 5664.
[8] Y.J. Li, X.M. Chen, R.Z. Hou, Y.H. Tang, Solid State Commun. 137 (2006) 120.
[9] Y.H. Lin, M. Li, C.W. Nan, J. Li, J. Wu, J. He, Appl. Phys. Lett. 89 (2006) 032907.
[10] S. Tangwancharoen, P. Thongbai, T. Yamwongb, S. Maensiria, Mater. Chem. Phys. 115 (2009) 585.
[11] W.M. Jadwisienczak, H.J. Lozykowski, A. Xu, B. Patel, J. Electron. Mater. 31 (2002) 776.
[12] W. Jia, K. Monge, F. Fernandez, Opt. Mater. 32 (2003) 27.
[13] Kenneth Barbalace, Periodic Table of Elements—Sorted by Ionic Radius (Environmental Chemistry), 1995–2008, http://EnvironmentalChemistry.com/yogi/periodic/ionicradius.html.
[14] G.-J. Chen, Y.-J. Hsiao, Y.-S. Chang, Y.-L. Chai, J. Alloys Compd. 474 (2009) 237.
[15] Powder Diffraction File, Joint Committee for Powder Diffraction Studies (JCPDS) file No.:02-1216.
[16] Z. Li, C. Wang, X. Ma, L.Y.J. Sun, Mater. Chem. Phys. 91 (2005) 36.
[17] M. Matsumiya, F. Qiu, W. Shin, N. Izu, N. Murayama, S. Kanzaki, Thin Solid Films 419 (2002) 213.
[18] E.F. Kaelble (Ed.), Handbook of X-rays for Diffraction, Emission, Absorption and Microscopy, McGraw-Hill, New York, 1967, pp. 17–25.
[19] D.P. Joseph, M. Saravanan, B. Muthuraaman, P. Renugambal, S. Sambasivam, S.P. Raja, P. Maruthamuthu, C. Venkateswaran, Nanotechnology 19 (2008) 485707.
[20] Y. Makino, S. Miyake, J. Alloys Compd. 313 (2000) 235.
[21] M. Ram, Solid State Commun. 149 (2009) 1226.
[22] R.M. Hill, A.K. Jonscher, J. Non-Cryst. Solids 32 (1979) 53.
[23] S.R. Elliott, Adv. Phys. 36 (1987) 135.
[24] R.H. Chen, R.Y. Chang, S.C. Shern, J. Phys. Chem. Solids 63 (2002) 2069.
[25] R.H. Chen, S.C. Shern, T. Fukami, J. Phys. Chem. Solids 63 (2002) 203.
[26] S.R. Elliot, J. Non-Cryst. Solids 35–36 (1980) 855.